photonics

MDPI

Article

Light Confinement with Structured Beams in Gold Nanoparticle Suspensions

Argelia Balbuena Ortega [1,2,*], Felix E. Torres-González [2], Valentin López Gayou [3], Raul Delgado Macuil [3], Gaetano Assanto [4] and Karen Volke-Sepulveda [2]

[1] Instituto de Energías Renovables, Universidad Nacional Autónoma de México, Priv. Xochicalco S/N Temixco, Morelos 62580, Mexico
[2] Instituto de Física, Universidad Nacional Autónoma de México, Ciudad de México 04510, Mexico; torresfelix@ciencias.unam.mx (F.E.T.-G.); karen@fisica.unam.mx (K.V.-S.)
[3] Instituto Politécnico Nacional—CIBA Tlaxcala, Km 1.5 Carretera Estatal Tecuexcomac-Tepetitla, Tepetitla de Lardizabal, Tlaxcala 90700, Mexico; vlopezg@ipn.mx (V.L.G.); rdmacuil@yahoo.com.mx (R.D.M.)
[4] NooEL—Nonlinear Optics and OptoElectronics Lab, University "Roma Tre", 00146 Rome, Italy; assanto@uniroma3.it
* Correspondence: abalbuena@ier.unam.mx

Abstract: We carry out an experimental campaign to investigate the nonlinear self-defocusing propagation of singular light beams with various complex structures of phase and intensity in a colloidal suspension of gold nanoparticles with a plasmonic resonance near the laser wavelength (532 nm). Studying optical vortices embedded in Gaussian beams, Bessel vortices and Bessel-cosine (necklace) beams, we gather evidence that while intense vortices turn into two-dimensional dark solitons, all structured wavepackets are able to guide a weak Gaussian probe of different wavelength (632.8 nm) along the dark core. The probe confinement also depends on the topological charge of the singular pump.

Keywords: nanocolloids; nanoparticles; soft-matter; nonlinear propagation; all-optical effects; opto-thermal effect; dark solitons; singular optics; nonlinear plasmonics; vortex beams; light self-localization; light-induced waveguides; structured beams

check for updates

Citation: Balbuena Ortega, A.; Torres-González, F.E.; López Gayou, V.; Delgado Macuil, R.; Assanto, G.; Volke-Sepulveda, K. Light Confinement with Structured Beams in Gold Nanoparticle Suspensions. *Photonics* **2021**, *8*, 221. https://doi.org/10.3390/photonics8060221

Received: 14 April 2021
Accepted: 10 June 2021
Published: 15 June 2021

Publisher's Note: MDPI stays neutral with regard to jurisdictional claims in published maps and institutional affiliations.

Copyright: © 2021 by the authors. Licensee MDPI, Basel, Switzerland. This article is an open access article distributed under the terms and conditions of the Creative Commons Attribution (CC BY) license (https://creativecommons.org/licenses/by/4.0/).

1. Introduction

The engineering of nanostructured materials has led to an important revolution across several disciplines, including medicine, biology, chemistry, optics and optoelectronics, materials science, and physics [1–4]. In photonics, in particular, the optical characteristics of materials have been tuned by properly tailoring size, shape and composition of the embedded nanostructures, as in the case of nanocolloids [5]. Specifically, colloidal suspensions of metallic nanoparticles (NP's) have shown to exhibit unique optical, electrical and catalytic properties, stimulating the research on various physical and chemical processes for their synthesis. In recent years, the risen interest in the development of environmentally friendly and sustainable preparation methods has drawn biosynthetic routes towards nanostructures with better defined sizes and morphologies as compared to physico-chemical techniques [6,7]. Among them, the NP synthesis based on plant extracts has been widely reported in the literature [8–10].

A few applications of metallic nanocolloids in photonics exploit their nonlinear optical response, which entails, for instance, the generation of self-confined wavepackets [5,6,11–16]. Since the Kerr-like (cubic) optical nonlinearity of nanocolloids can be either positive (focusing) or negative (defocusing) depending on the NP size and the wavelength of light, the generation of bright or dark spatial solitons has been pursued with them, as well, using pulsed or continuous-wave (CW) excitations [5,13]. The availability of such assortment of tunable all-optical materials has furthered all-optical circuits inspired

by the "light guiding light" paradigm, whereby control beams are employed to switch, guide and/or modulate information-carrying wavepackets in photonic networks based on solitary waves and their interactions [17–27].

Bright spatial solitons can be generated in Kerr-like nonlinear media with a positive light-induced refractive index increase; conversely, dark solitons are self-trapped beams due to a repulsive (self-defocusing) nonlinearity [18,20,28,29]. Early experiments on dark solitons reported stripe solitary waves [30,31]; a probe could be injected and guided by a dark stripe [32], and steered by adjusting the relative phase between waves at either sides [33].

In two transverse dimensions, (2+1)D dark optical solitons with a black core are often addressed as vortex solitons [29]. The profile of an optical vortex beam consists of a dark (black) core surrounded by a bright background or annulus, its zero intensity on axis coinciding with a screw-type phase singularity [34]; the wavefronts of a vortex are m intertwined rotating helices, with m an integer termed winding number or topological charge. In the linear regime, the singularity preserves in propagation but the dark core broadens owing to diffraction. In self-defocusing media the core spreading can be balanced out by the higher refractive index on axis, resulting in a vortex soliton and a waveguide for the confinement of additional (weak) signals [29,35,36]. Guided waves supported by (2+1)D vortex solitons have been reported, e.g., in photorefractives [37,38] and nanocolloids [12].

Nonlinear light beams with a more complex field structure, including Bessel beams, multipole solitons and necklace beams, have also been addressed [39–44]. For example, zeroth-order Bessel beams in a weakly self-focusing medium or propagating in the presence of attractive/repulsive Kerr responses were investigated by Gadonas et al. [39] and by Johannisson et al. [40], respectively. Although other features of vortices and vortex solitons in conjunction with Bessel beams in self-defocusing media have been studied [45,46], to date most experiments using singular CW beams with complex phase and intensity structure have been conducted with positive nonlinearities yielding self-focusing [47–53].

In this paper, extending and completing our initial investigation [16], we report on propagation and guiding of various dark-cored CW singular beams through a colloidal suspension of gold nanoparticles exhibiting a repulsive, polarization-independent, nonlinearity. The latter stems from the opto-thermal response associated with linear absorption of the laser light (532 nm) near a plasmonic resonance. Following a summary of the technological process involved in the "green" preparation of the soft-matter suspension, we specifically study annular vortex beams with no radial structure and Bessel vortices with multi-annular morphology, both of them encompassing orbital angular momentum, as well as Bessel-cosine beams, a type of necklace mode. All such patterns were created using a spatial light modulator (SLM) to prepare appropriate phase masks. Light-induced incoherent confinement was examined with a pump-probe scheme, collinearly injecting a weaker Gaussian beam of wavelength 632.8 nm in the dark region of each singular beam. At variance with earlier reports [16], we also analyze the role of the winding number in the formation of solitons and waveguides with these complex wavepackets.

2. Material and Methods

2.1. Nanoparticle Synthesis

The metal nanoparticles suspended in our colloid were prepared by a green synthesis process or biosynthesis. The latter relied on the *Bacopa procumbens* plant from "Centro de Investigación en Biotecnología Aplicada-IPN, Mexico" and is illustrated in the schematic synopsis of Figure 1a. An essence was produced with the powder (40 g) obtained from drying and grinding the plant, adding it to 600 mL of hydro-alcoholic solution (50:50 water:ethylene). This underwent reflux for 4 h, and the extracted liquid was first centrifuged at 2000 rpm for 10 min, then filtered and concentrated by low-pressure distillation using a rotary evaporator. The semi-solid condensate was finally dried under vacuum to yield the hydro-alcoholic extract. After preparation, the latter was diluted with deionized water in the ratio 1mg:1ml. A chloro-auric solution (analytic grade $HAuCl_4$ from Sigma-Aldrich)

diluted at 1 mM in deionized water was mixed with the *Bacopa procumbens* extract in a 7:3 volume ratio and allowed to react for two hours at room temperature. The gold nanoparticles obtained were finally characterized by transmission electron microscopy (TEM), resulting quasi-spherical with an approximate diameter of 5 nm. Figure 1b shows the measured UV-vis normalized absorbance spectrum, with an inset displaying a TEM image of the biosynthesized gold nanocolloid (BGN).

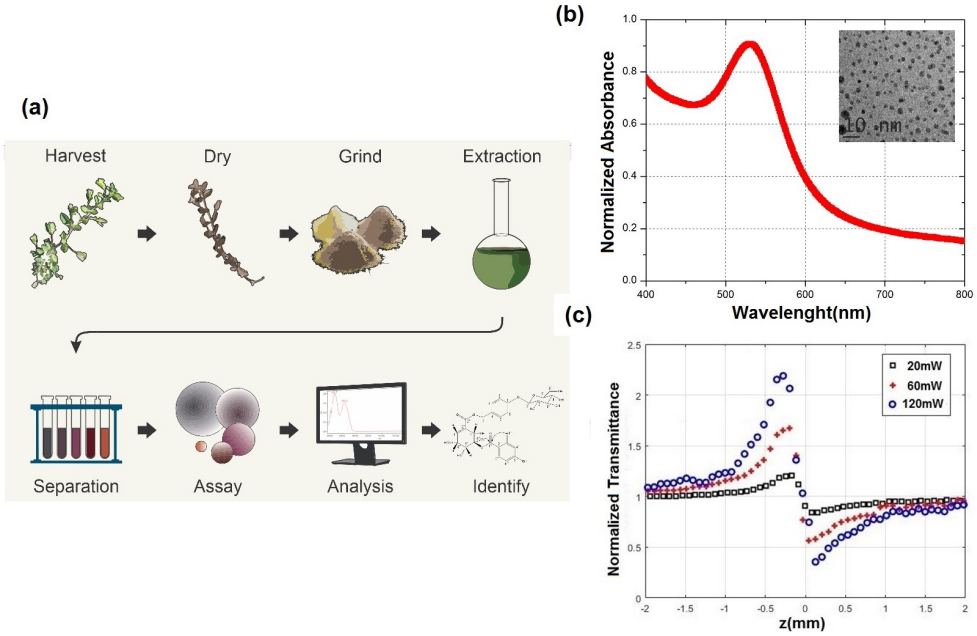

Figure 1. (**a**) Visual synopsis of the green synthesis method for gold nanocolloid preparation. (**b**) UV-vis normalized absorbance of the suspension versus wavelength; the inset is a TEM image of the nanoparticles. (**c**) z-scan data points showing the nonlinear transmission of the sample at $\lambda = 532$ nm in the close aperture mode for various beam powers, as specified in the legend.

2.2. Nonlinearity: z-Scan Analysis

The nonlinear optical response of the BGN was measured with the z-scan technique [54], employing a CW Gaussian laser beam at $\lambda = 532$ nm (i.e., the pump in the experiments described in the next section). The beam was focused on the sample by a convex lens, yielding a waist of 4.5 µm, with a Rayleigh range of 120 µm. To determine the nonlinear changes in refractive index by z-scan in the close-aperture mode, the normalized transmittance was acquired with a photodetector after a circular aperture (1 mm radius) placed at 90 cm from the cell exit, varying the sample location along the axis z of light propagation. The results of the close-aperture z-scan are plotted in Figure 1c for various incident powers. A transmittance peak followed by a minimum indicates a self-defocusing (repulsive) nonlinear optical response. The nonlinear absorption, characterized via open-aperture z-scan, was found to be negligible, consistently with the results from similar colloids containing larger gold nanoparticles [14]. Conversely, the linear UV-vis absorption, graphed in Figure 1b, showed a peak close to the laser wavelength $\lambda = 532$ nm. The latter resonance suggests a temperature-driven all-optical response due to the heat from power dissipation. By fitting a nonlocal model to the acquired z-scan curves, as detailed in Ref. [15], we were able to estimate a Kerr-like coefficient for the intensity-dependent refractive index of $n_2 = -1.84 \times 10^{-12}$ m^2/W, with a cubic susceptibility $\chi^{(3)} = -1.28 \times 10^{-14}$ m^2/V^2. We also performed z-scan at the wavelength of the probe $\lambda = 632.8$ nm, but the quantitative results were rather insignificant as compared with those from the pump.

It should be stressed that optical trapping forces, playing an important role in the nonlinear properties of other nanocolloids [5,25], are negligible in the present kind of

samples [14–16]), owing to the dominant opto-thermal effect and the reduced size of the nanoparticles in the BGN; optical trapping on small particles, in fact, tends to be proportional to their volume [55].

2.3. Experimental Set-Up and Characterization

For the experiments, a linearly polarized CW Gaussian beam ($\lambda = 532$ nm) with waist radius of 1.69 mm impinged onto a reflecting SLM, programmed with various phase masks in order to generate the structured singular wavepackets of interest. The simplest profiles were Gaussian-embedded vortices with topological charges $m = 1$ and $m = 2$, respectively, carrying orbital angular momentum (OAM) [56]; these beams will be referred to as simple vortices (SV's). The complex amplitude of the electric field at the waist of the Gaussian envelope is described by

$$E_{SV}(\mathbf{r}) = A \exp\left(-\rho^2/w^2\right) \exp\left(im\varphi\right), \tag{1}$$

where $\mathbf{r} = (\rho, \varphi)$ with $\rho = \sqrt{x^2 + y^2}$ and $\varphi = \arctan\left(y/x\right)$ the radial and azimuthal cylindrical coordinates, respectively. The SV above carries an OAM of $\hbar m$ per photon but, at variance with structurally stable Laguerre-Gauss profiles, propagating for $z > 0$ it shows a rapidly diffracting dark core surrounded by bright (progressively dimmer) concentric annular rings [57]. We also formed OAM-carrying Bessel-Gauss vortices with $m = 1$ and $m = 2$, which at the waist can be cast as:

$$E_{BV}(\mathbf{r}) = A \exp\left(-\rho^2/w^2\right) J_m(k_t r) \exp\left(im\varphi\right), \tag{2}$$

with $J_m(\cdot)$ the ordinary Bessel function of order m and k_t denoting the transverse component of the wave-vector. Finally, we prepared Bessel-cosine or necklace beams described by:

$$E_{BC}(\mathbf{r}) = A \exp\left(-\rho^2/w^2\right) J_m(k_t r) cos(m\varphi). \tag{3}$$

In the latter case, we set $m = 2$ and $m = 3$, aiming to obtain symmetric dark cores as in SV's and BV's. All the structured beams above have a dark core on-axis, a black (non-illuminated) region to be exploited in the self-defocusing regime for its higher refractive index with respect to the surroundings.

The experimental setup is sketched in Figure 2a. After the SLM, the structured pump was collimated and reduced in size using a $4f$ telescope (L1-MO). Lens L1 had a 40 cm focal length and the 10× microscope objective a numerical aperture NA = 0.25. The Gaussian envelope had a waist of ∼85 µm after the telescope, corresponding to a Rayleigh range >55 mm. Varying the beam power P in the range 30–125 mW, in this geometry the input intensity ranged from 1.3×10^6 to 5.5×10^6 W/m^2, respectively (powers below 30 mW yielded unobservant nonlinear effects).

A CW laser probe ($\lambda_r = 632.8$ nm), with Gaussian profile and power ≤19 mW, was made collinear with the pump and focused on a waist of 18 µm (in air), entering the BGN in the same linear polarization of the singular beam. The BGN filled a home-made transparent cuvette of dimensions 2 mm along x (thickness), 5 mm along y (width) and 10 mm along z (length), respectively, mounted on a translation stage along the beam axis (z) in order to optimize the phase-front curvature of the probe to be launched in the core of the structured pump. The Gaussian envelope of the latter was essentially collimated over the sample length. The imaging systems VS1 and VS2 were employed to observe the evolution of the pump and its effects on the probe both during and after propagation. The first one (VS1), consisting of a microscope objective (10×, NA = 0.40) and a color CCD camera, helped characterizing the transverse profiles of both pump and probe at the output. The second one (VS2) provided a side-view along the propagation by imaging the scattered light [58]; it combined two perpendicularly oriented cylindrical lenses with focal lengths 10 cm (z-axis) and 5 cm (y-axis) to obtain images with magnifications 6.8 and 0.5,

respectively. Narrow-band interference filters in both detection systems separated pump and probe photons.

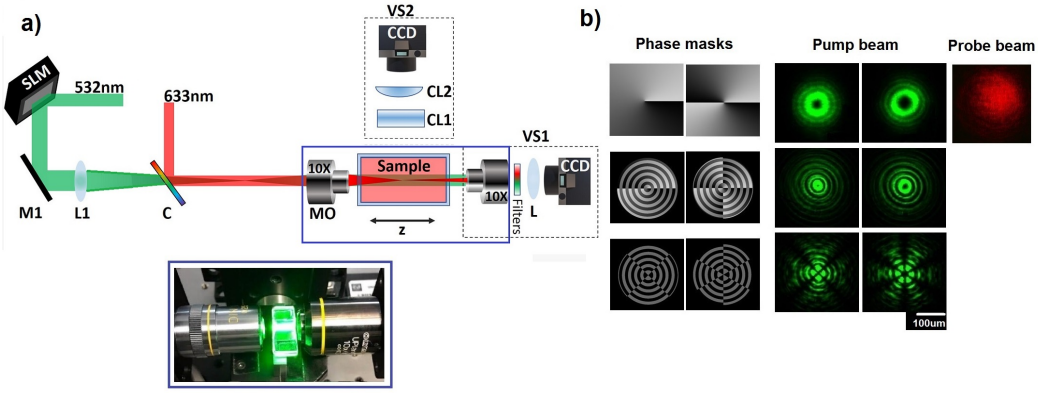

Figure 2. (**a**) Experimental set-up. SLM: phase-only spatial light modulator; M1: mirror; L1: convex lens; C: beam combiner; MO: microscope objective; VS1–VS2: visualization systems. VS1 includes a 10× microscope objective and a convex lens (L), while VS2 combines a pair of perpendicularly oriented cylindrical lenses (CL1, CL2); in both cases images were recorded with color CCD cameras. The photograph below shows the laser illuminated cuvette between MO's. (**b**) Left: various phase masks programmed in the SLM; center: corresponding transverse intensity profiles of the pump at the sample input; right: transverse intensity of the probe at the input. The same scaling applies to the images of all beams.

3. Results and Discussion

In contrast with earlier reports on silver NP's in acetone, a nanocolloid with third-order (linearly dependent on intensity) repulsive and fifth-order (quadratically dependent on intensity) positive nonlinearities competing with one another [12], our BGN suspension was exclusively self-defocusing for the pump. While it was previously believed that fifth-order focusing was a crucial ingredient of the Kerr-like response to support stable light-induced waveguides, as we demonstrate in the following the BGN material provided stable confinement, not only with ring-shaped vortices, but with all the singular beams. Moreover, the maximum intensity employed in our experiments was five orders of magnitude lower than that employed in silver nanocolloids [12], indicating a significantly larger nonlinearity owing to a plasmon resonance at the pump wavelength.

In previous studies of gold nanocolloids [11,14,15], it was recognized how, even for NP mean diameter (40 nm) considerably larger than in this work, thermo-mediated self-defocusing dominated over potential self-focusing contributions due to optical trapping [14]. Therefore, it was expected that no NP redistribution would be caused by the incident beam, backing up the measured evidence of lacking nonlinear absorption [14,15]. When focusing a bell-shaped Gaussian beam (with a single lens rather than a $4f$ telescope) in such colloid, the focal plane (waist location) moved forward and the spot widened, with a reduction of the overall divergence versus input power [14,15]. Although the propagation of a (weaker) probe could be controlled by such a lens-like defocusing and apparent self-collimation, it did not relate to the formation of a waveguide [15], as the nonlinear refractive index lowered instead of increasing along the beam axis. Scalar and vector vortices preserved their intensity and polarization structure with a seemingly diffraction-free propagation, similar to the Gaussian case just described, but always due to pump focusing inside the sample [14]. On the contrary, in order to look for dark solitons and all-optical waveguides in the dark region on-axis, hereby we injected a vortex beam (i.e., a non-structurally stable singular beam, see Equation (1)) with a dark core rapidly diffracting despite the outer envelope remained nearly collimated along the whole cuvette length in the linear regime, as illustrated in Figure 3. After the image plane, in the nonlinear regime the dark core self-confined while the envelope self-diverged.

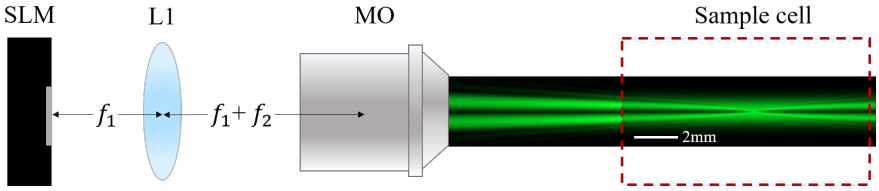

Figure 3. Sketch of the $4f$ telescope after the SLM (out of scale), including the simulated linear propagation of the SV past the microscope objective (in scale). The location of the sample cell is framed by a dashed box; in the image plane the dark core appears to vanish.

Figure 4 presents transverse profile images of the superposed pump and probe beams at the sample output for pump powers of 30 mW and 125 mW and six input structures: embedded vortex (SV) with $m = 1, 2$; Bessel vortex (BV) with $m = 1, 2$ and Bessel cosine (BC) with $m = 2, 3$. The rightmost photographs for each singular structure display the probe only (filtered out pump). In both SV instances (left panels), the outer profile expanded versus power, as expected. However, while the dark core kept approximately the same size for $m = 1$, it slightly narrowed for $m = 2$, suggesting that self-defocusing prevailed over diffraction at the highest power level.

For BV and BC wavepackets (center and right panels, respectively), the whole transverse intensity distribution scaled up in size versus power, regardless of the winding number m. Such finding is in agreement with the theoretical results reported for the zeroth-order Bessel beam propagating in a self-defocusing medium [40]. Both BV and BC beams were slightly deformed at the output, with the upper part of the profile wider than the lower one. This can be attributed to convection currents in the BGN suspension due to the absorption-mediated temperature increase.

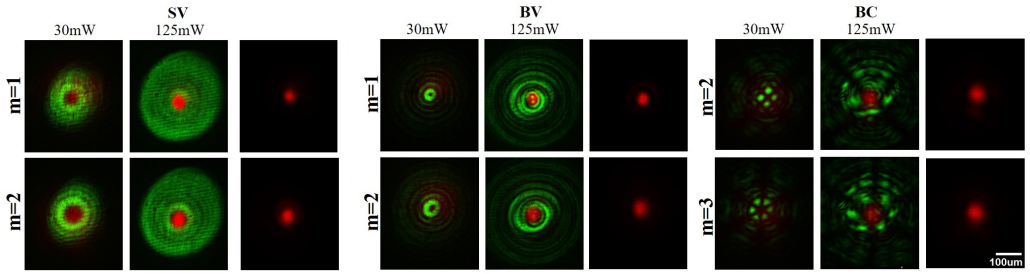

Figure 4. Acquired transverse profiles of pump ($\lambda_g = 532$ nm) at the sample exit for input pump powers $P = 30$ and $P = 125$ mW, and the probe ($\lambda_r = 632.8$ nm) for the various singular input structures and a pump power of 125 mW. (Left) Simple vortex with $m = 1$ (top) and $m = 2$ (bottom); (center) Bessel vortex with $m = 1$ (top) and $m = 2$ (bottom); (right) Bessel-cosine with $m = 2$ (top) and $m = 3$ (bottom). The rightmost photographs in each block display the probe profile after filtering out the pump.

The probe profile at the output allowed us to gain insight onto the pump evolution within the sample. In all cases, the probe output spot narrowed versus pump excitation. At $P = 125$ mW the Gaussian probe matched the size of the dark core independent of the pump structure and its topological charge. Remarkably, the red signal guided by and along the singularity remained bell-shaped despite the various levels of azimuthal complexity and dark-core diameter of the structured inputs. This result indicates the presence of a graded, bell-shaped refractive index distribution in the transverse plane, maximum on axis due to the repulsive nonlinearity and irrespective of the specific intensity patterns, the latter with smaller features in BV's and BC's than in SV's. The formation of a smooth bell-shaped potential is ascribed to the substantial medium nonlocality, as a highly nonlocal nonlinear response is expected to filter out the fine details of the excitation and mimic its widened envelope [59].

At the highest pump power the output probe shrank between 2.5 and 5 times with respect to the input, depending on the topological charge. This can be appreciated from Figure 5, plotting the measured probe diameter at the sample exit versus pump power for the various structures and winding numbers. Lower topological charges (m) resulted into a more tightly confined probe, owing to narrower dark cores. In particular, the probe size reduced to one fifth in $m = 1$ BV's (i.e., structures with the smallest core), while it reduced to about 40% in $m = 3$ BC's (with the widest core). We stress that the nonlinear response of the red probe was too weak to affect the pump-induced waveguide in the explored power range [16].

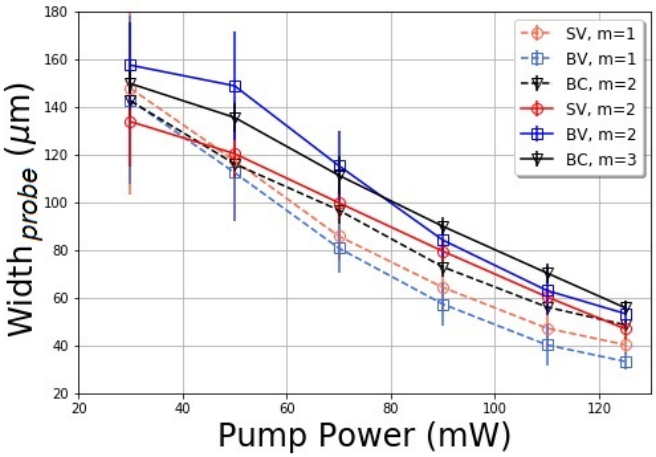

Figure 5. Measured diameter of the probe output versus input pump power for the singular structures in Figure 2b, with winding numbers as specified in the legend.

The probe evolution along the cell was monitored with the aid of VS2, imaging the light scattered on the side. Typical results are reported in Figure 6 for a BV with $m = 1$ (please note the different scales for propagation (z) and transverse (y) coordinates). We observed that the pump-induced waveguide did not form right at the entrance of the sample, and that the probe coupling depended on both pump structure and power. Hence, by adjusting the cell position along z we could optimize the probe coupling to the confining core of each structured profile and excitation level. To clearly observe the nonlinear evolution of the beams throughout the entire propagation length despite the high scattering losses, in fact, the image plane of the pump structure was not positioned at the entrance of the cuvette but within the sample. Therefore, the dark core narrowed from the input up to the image plane, and the probe had to be focused accordingly in order to be coupled to the induced waveguide (see Figure 3).

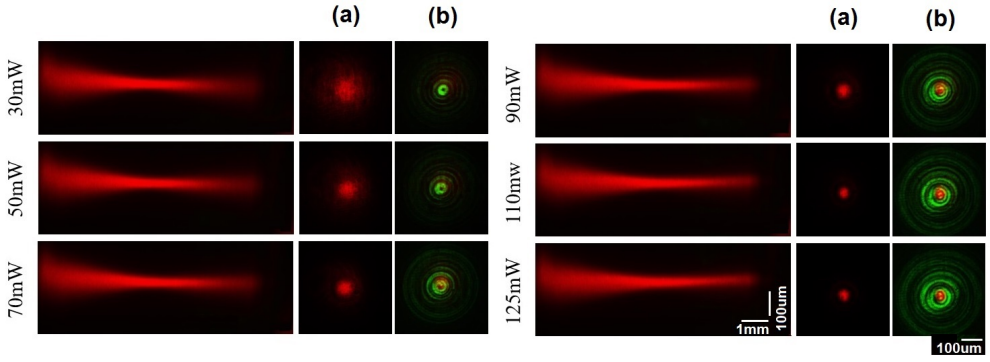

Figure 6. Propagation of the red probe collinear with $m = 1$ BV for various input powers, as labeled on the vertical axes. Leftmost photographs in each panel: x-z evolution along the sample. (**a**) Transverse intensity profile of red probe at the output; (**b**) superimposed transverse intensity profiles of the red probe and the green pump at the output.

4. Conclusions

We prepared a colloidal suspension of bio-synthesized gold nanoparticles and characterized its one-photon (UV-vis) spectral absorbance, as well as its nonlinear Kerr-like optical response by both close and open aperture z-scan. Employing laser light of wavelength 532 nm close to a plasmonic resonance, we investigated the nonlinear self-defocusing propagation of three kinds of singular beams with dark core: OAM-carrying annular vortices embedded in Gaussian beams and Bessel vortices, and Bessel-cosine necklaces. In all instances, when exciting the opto-thermal repulsive response, the size of the dark cores depended on the input power and the topological charge (m) of the structured input. Annular vortices with $m = 1$ evolved with an invariant core along the propagation length, while their surrounding bright ring broadened versus power, indicating the formation of a two-dimensional dark soliton. For $m = 2$ and high excitation power, the dark core of the simple vortex seemed slightly narrowed towards the end of the cell, suggesting that self-defocusing dominated over spatial dispersion. Bessel vortices and Bessel-cosine beams, with higher complexity across both radial and azimuthal coordinates, showed a nearly uniform broadening versus propagation, except for minor deformations probably due to thermal convection.

By launching a weaker Gaussian beam at 632.8 nm collinear with the singular structures at 532 nm in a pump-probe scheme, we could investigate the transverse confinement afforded by self-effects near plasmon resonance. In all cases in the nonlinear regime, the dark-cored pump gave rise to graded-index waveguides for the red signal, with lower topological charges favoring its transverse trapping. The guided probe remained bell-shaped irrespective of the pump structure, indicating a strongly nonlocal all-optical response, mainly caused by heat diffusion from the metal nanoparticles. In fact, the radial and azimuthal nodes of either Bessel beams played no role on the output probe profile, indicating that the light-induced refractive index distribution was smooth and did not reproduce the fine pump structure. Moreover, since the dark cores of Bessel vortex and necklace beams were initially much narrower than those of ring-shaped vortices, their Gaussian envelopes appeared to determine the shape of the BGN response, the latter acting as a negative lens and magnifying the whole wavepackets. Once dark-core diffraction was balanced by defocusing, the light-induced bell-shaped refractive index distribution with maximum on-axis could guide the probe. The latter was best coupled into the nonlinear waveguide when matching the transverse extent of the dark-core. A more detailed characterization of this phenomenon is in progress as it might provide useful information on the range of non-locality.

The results presented and summarized above disclose several new features of self-localization and signal cross-guidance using structured beams with/without orbital angular momentum in self-defocusing media, a step forward in "light guiding light" scenarios. The optical properties of colloidal suspensions with biosynthesized gold nanoparticles, exploited in this experimental work, appear to be well suited for soft-matter nonlinear photonics with solitary waves, despite some power dissipation. Finally, the engineering of colloidal suspensions with plasmonic nanoparticles of various sizes entailing the competition between Kerr-like nonlinearities of opposite signs might lead -in the near future- to demonstrating novel effects in such media. These could include, among others, thermal control of soliton routing [60,61] as well as multi-peaked supermode solitons in scalar and vector formats [62,63].

Author Contributions: Conceptualization, A.B.O., K.V.-S. and G.A.; sample preparation, V.L.G. and R.D.M.; experiments and formal analysis, A.B.O. and F.E.T.-G.; investigation, all authors; writing—original draft preparation A.B.O. and K.V.-S.; writing—review and editing, G.A.; project administration and funding acquisition, K.V.-S. All authors have read and agreed to the published version of the manuscript.

Funding: Project partially supported by DGAPA-UNAM (grant PAPIIT IN113419).

Institutional Review Board Statement: Not applicable.

Informed Consent Statement: Not applicable.

Data Availability Statement: The data that support the findings of this study are available from the corresponding author upon reasonable request.

Acknowledgments: A. Balbuena Ortega acknowledges support from Cátedras CONACyT. We thank Alejandro V. Arzola for useful discussions.

Conflicts of Interest: The authors declare no conflict of interest.

Abbreviations

The following abbreviations are used in this manuscript:

NP	Metal Nanoparticles
CW	Continuous Wavelength
BGN	Bio-synthesized Gold Nanoparticles
TEM	Transmission Electron Microscope
SLM	Spatial Light Modulator
OAM	Optical Angular Momentum
MO	Microscope Objective
C	(Beam) Combiner
CCD	Charge Coupled Device
SV	Simple Vortex
BV	Bessel Vortex
BC	Bessel-Cosine
VS1	Visualisation System 1
VS2	Visualisation System 2

References

1. Wilson, M.; Kannangara, K.; Smith, G.; Simmons, M.; Raguse, B. *Nanotechnology: Basic Science and Emerging Technologies*; CRC Press: Boca Raton, FL, USA, 2002.
2. Roco, M.C.; Mirkin, C.A.; Hersam, M.C. Nanotechnology Research Directions for Societal Needs in 2020: Summary of International Study. *J. Nanopart. Res.* **2011**, *13*, 897–919. [CrossRef]
3. Boisseau, P.; Loubaton, B. Nanomedicine, nanotechnology in medicine. *C. R. Phys.* **2011**, *12*, 620–636. [CrossRef]
4. Rogers, B.; Adams, J.; Pennathur, S. *Nanotechnology: Understanding Small Systems*; CRC Press: Boca Raton, FL, USA, 2014.
5. Fardad, S.; Salandrino, A.; Heinrich, M.; Zhang, P.; Chen, Z.; Christodoulides, D.N. Plasmonic resonant solitons in metallic nanosuspensions. *Nano Lett.* **2014**, *14*, 2498–2504. [CrossRef]
6. Sathyavathi, R.; Krishna, M.B.; Rao, S.V.; Saritha, R.; Rao, D.N. Biosynthesis of silver nanoparticles using Coriandrum sativum leaf extract and their application in nonlinear optics. *Adv. Sci. Lett.* **2010**, *3*, 138–143. [CrossRef]
7. Begum, N.A.; Mondal, S.; Basu, S.; Laskar, R.A.; Mandal, D. Biogenic synthesis of Au and Ag nanoparticles using aqueous solutions of Black Tea leaf extracts. *Coll. Surf. B Biointerfaces* **2009**, *71*, 113–118. [CrossRef] [PubMed]
8. Marchiol, L. Synthesis of metal nanoparticles in living plants. *It. J. Agron.* **2012**, *7*, 274–282. [CrossRef]
9. Gardea-Torresdey, J.L.; Gomez, E.; Peralta-Videa, J.R.; Parsons, J.G.; Troiani, H.; Jose-Yacaman, M. Alfalfa sprouts: A natural source for the synthesis of silver nanoparticles. *Langmuir* **2003**, *19*, 1357–1361. [CrossRef]
10. Park, Y.; Hong, Y.; Weyers, A.; Kim, Y.; Linhardt, R. Polysaccharides and phytochemicals: A natural reservoir for the green synthesis of gold and silver nanoparticles. *IET Nanobiotechnol.* **2011**, *5*, 69–78. [CrossRef] [PubMed]
11. Souza, R.F.; Alencar, M.A.; da Silva, E.C.; Meneghetti, M.R.; Hickmann, J.M. Nonlinear optical properties of Au nanoparticles colloidal system: Local and nonlocal responses. *Appl. Phys. Lett.* **2008**, *92*, 201902. [CrossRef]
12. Reyna, A.S.; De Araujo, C.B. Guiding and confinement of light induced by optical vortex solitons in a cubic–quintic medium. *Opt. Lett.* **2016**, *41*, 191–194. [CrossRef] [PubMed]
13. Kelly, T.S.; Ren, Y.X.; Samadi, A.; Bezryadina, A.; Christodoulides, D.; Chen, Z. Guiding and nonlinear coupling of light in plasmonic nanosuspensions. *Opt. Lett.* **2016**, *41*, 3817–3820. [CrossRef]
14. Shvedov, V.; Cyprych, K.; Salazar-Romero, M.Y.; Izdebskaya, Y.; Krolikowski, W. Nonlinear propagation and quasi self-confinement of light in plasmonic resonant media. *Opt. Express* **2018**, *26*, 23196–23206. [CrossRef]
15. Balbuena Ortega, A.; Brambila, E.; López Gayou, V.; Delgado Macuil, R.; Orduña Diaz, A.; Zamilpa Alvarez, A.; Arzola, A.; Volke-Sepúlveda, K. Light control through a nonlinear lensing effect in a colloid of biosynthesized gold nanoparticles. *J. Mod. Opt.* **2019**, *66*, 502–511. [CrossRef]
16. Balbuena Ortega, A.; Torres-González, F.; López Gayou, V.; Delgado Macuil, R.; Cardoso Sakamoto, J.; Arzola, A.; Assanto, G.; Volke-Sepulveda, K. Guiding light with singular beams in nanoplasmonic colloids. *Appl. Phys. Lett.* **2021**, *118*, 061102. [CrossRef]

17. Snyder, A.W.; Ladouceur, F. Light Guiding Light: Letting Light Be the Master of Its Own Destiny. *Opt. Photon. News* **1999**, *10*, 35. [CrossRef]
18. Stegeman, G.I.; Segev, M. Optical spatial solitons and their interactions: Universality and diversity. *Science* **1999**, *286*, 1518–1523. [CrossRef] [PubMed]
19. Assanto, G.; Fratalocchi, A.; Peccianti, M. Spatial solitons in nematic liquid crystals: From bulk to discrete. *Opt. Express* **2007**, *15*, 5248–5259. [CrossRef]
20. Chen, Z.; Segev, M.; Christodoulides, D.N. Optical spatial solitons: Historical overview and recent advances. *Rep. Progress Phys.* **2012**, *75*, 086401. [CrossRef]
21. Snyder, A.W.; Sheppard, A. Collisions, steering, and guidance with spatial solitons. *Opt. Lett.* **1993**, *18*, 482–484. [CrossRef]
22. Fratalocchi, A.; Piccardi, A.; Peccianti, M.; Assanto, G. Nonlinearly controlled angular momentum of soliton clusters. *Opt. Lett.* **2007**, *32*, 1447–1449. [CrossRef]
23. Piccardi, A.; Alberucci, A.; Bortolozzo, U.; Residori, S.; Assanto, G. Soliton gating and switching in liquid crystal light valve. *Appl. Phys. Lett.* **2010**, *96*, 071104. [CrossRef]
24. Izdebskaya, Y.V.; Rebling, J.; Desyatnikov, A.; Assanto, G.; Kivshar, Y.S. All-optical switching of a signal by a pair of interacting nematicons. *Opt. Express* **2012**, *20*, 24701–24707. [CrossRef] [PubMed]
25. Salazar-Romero, M.Y.; Ayala, Y.A.; Brambila, E.; Lopez-Peña, L.A.; Sciberras, L.; Minzoni, A.A.; Terborg, R.A.; Torres, J.P.; Volke-Sepúlveda, K. Steering and switching of soliton-like beams via interaction in a nanocolloid with positive polarizability. *Opt. Lett.* **2017**, *42*, 2487–2490. [CrossRef] [PubMed]
26. Perumbilavil, S.; Piccardi, A.; Barboza, R.; Buchnev, O.; Kauranen, M.; Strangi, G.; Assanto, G. Beaming random lasers with soliton control. *Nat. Commun.* **2018**, *9*, 3863. [CrossRef] [PubMed]
27. Assanto, G. Nematicons: Reorientational solitons from optics to photonics. *Liq. Cryst. Rev.* **2018**, *6*, 170–194. [CrossRef]
28. Kivshar, Y.S.; Luther-Davies, B. Dark optical solitons: Physics and applications. *Phys. Rep.* **1998**, *298*, 81–197. [CrossRef]
29. Desyatnikov, A.; Torner, L.; Kivshar, Y. Optical vortices and vortex solitons. *Prog. Opt.* **2005**, *47*, 1–60.
30. Andersen, D.R.; Hooton, D.E.; Swartzlander, G.A.; Kaplan, A.E. Direct measurement of the transverse velocity of dark spatial solitons. *Opt. Lett.* **1990**, *15*, 783–785. [CrossRef] [PubMed]
31. Allan, G.; Skinner, S.; Andersen, D.; Smirl, A.L. Observation of fundamental dark spatial solitons in semiconductors using picosecond pulses. *Opt. Lett.* **1991**, *16*, 156–158. [CrossRef]
32. Luther-Davies, B.; Xiaoping, Y. Waveguides and Y junctions formed in bulk media by using dark spatial solitons. *Opt. Lett.* **1992**, *17*, 496–498. [CrossRef]
33. Luther-Davies, B.; Yang, X. Steerable optical waveguides formed in self-defocusing media by using dark spatial solitons. *Opt. Lett.* **1992**, *17*, 1755–1757. [CrossRef]
34. Nye, J.F.; Berry, M.V. Dislocations in wave trains. *Proc. R. Soc. Lond. A Math. Phys. Sci.* **1974**, *336*, 165–190.
35. Snyder, A.; Poladian, L.; Mitchell, D. Stable black self-guided beams of circular symmetry in a bulk Kerr medium. *Opt. Lett.* **1992**, *17*, 789–791. [CrossRef] [PubMed]
36. Swartzlander, G., Jr.; Law, C. Optical vortex solitons observed in Kerr nonlinear media. *Phys. Rev. Lett.* **1992**, *69*, 2503. [CrossRef] [PubMed]
37. Chen, Z.; Segev, M.; Christodoulides, D.N.; Feigelson, R.S. Waveguides formed by incoherent dark solitons. *Opt. Lett.* **1999**, *24*, 1160–1162. [CrossRef]
38. Passier, R.; Chauvet, M.; Wacogne, B.; Devaux, F. Light-induced waveguide by a finite self-trapped vortex beam in a photorefractive medium. *J. Opt.* **2011**, *13*, 085502. [CrossRef]
39. Gadonas, R.; Jarutis, V.; Paškauskas, R.; Smilgevičius, V.; Stabinis, A.; Vaičaitis, V. Self-action of Bessel beam in nonlinear medium. *Opt. Commun.* **2001**, *196*, 309–316. [CrossRef]
40. Johannisson, P.; Anderson, D.; Lisak, M.; Marklund, M. Nonlinear Bessel beams. *Opt. Commun.* **2003**, *222*, 107–115. [CrossRef]
41. Rotschild, C.; Cohen, O.; Manela, O.; Segev, M.; Carmon, T. Solitons in nonlinear media with an infinite range of nonlocality: first observation of coherent elliptic solitons and of vortex-ring solitons. *Phys. Rev. Lett.* **2005**, *95*, 213904. [CrossRef]
42. Porras, M.A.; Parola, A.; Faccio, D.; Dubietis, A.; Di Trapani, P. Nonlinear unbalanced Bessel beams: Stationary conical waves supported by nonlinear losses. *Phys. Rev. Lett.* **2004**, *93*, 153902. [CrossRef]
43. Maleshkov, G.; Neshev, D.N.; Dreischuh, A. Nonlinear beam steering by fractional vortex dipoles. *Phys. Rev. A* **2009**, *80*, 053828. [CrossRef]
44. Jukna, V.; Milián, C.; Xie, C.; Itina, T.; Dudley, J.; Courvoisier, F.; Couairon, A. Filamentation with nonlinear Bessel vortices. *Opt. Express* **2014**, *22*, 25410–25425. [CrossRef] [PubMed]
45. Porras, M.A.; Ramos, F. Quasi-ideal dynamics of vortex solitons embedded in flattop nonlinear Bessel beams. *Opt. Lett.* **2017**, *42*, 3275–3278. [CrossRef] [PubMed]
46. García-Riquelme, J.L.; Ramos, F.; Porras, M.A. Optical vortex trapping and annihilation by means of nonlinear Bessel beams in nonlinear absorbing media. *J. Opt. Soc. Am. B* **2018**, *35*, 3030–3038. [CrossRef]
47. Stoyanov, L.; Dimitrov, N.; Stefanov, I.; Neshev, D.; Dreischuh, A. Optical waveguiding by necklace and azimuthon beams in nonlinear media. *J. Opt. Soc. Am. B* **2017**, *34*, 801–807. [CrossRef]
48. Rose, P.; Boguslawski, M.; Denz, C. Nonlinear lattice structures based on families of complex nondiffracting beams. *New J. Phys.* **2012**, *14*, 033018. [CrossRef]

49. Izdebskaya, Y.; Assanto, G.; Krolikowski, W. Observation of stable-vector vortex solitons. *Opt. Lett.* **2015**, *40*, 4182–4185. [CrossRef] [PubMed]
50. Izdebskaya, Y.V.; Shvedov, V.G.; Jung, P.S.; Krolikowski, W. Stable vortex soliton in nonlocal media with orientational nonlinearity. *Opt. Lett.* **2018**, *43*, 66–69. [CrossRef]
51. Laudyn, U.A.; Kwaśny, M.; Karpierz, M.A.; Assanto, G. Vortex nematicons in planar cells. *Opt. Express* **2020**, *28*, 8282–8290. [CrossRef] [PubMed]
52. Kwaśny, M.; Karpierz, M.A.; Assanto, G.; Laudyn, U.A. Optothermal vortex-solitons in liquid crystals. *Opt. Lett.* **2020**, *45*, 2451–2453. [CrossRef]
53. Brzobohatỳ, O.; Chvátal, L.; Šiler, M.; Zemánek, P. Complex colloidal structures with non-linear optical properties formed in an optical trap. *Opt. Express* **2020**, *28*, 37700–37707. [CrossRef]
54. Sheik-Bahae, M.; Said, A.A.; Wei, T.H.; Hagan, D.J.; Van Stryland, E.W. Sensitive measurement of optical nonlinearities using a single beam. *IEEE J. Quantum Electron.* **1990**, *26*, 760–769. [CrossRef]
55. Ashkin, A.; Dziedzic, J.M.; Bjorkholm, J.E.; Chu, S. Observation of a single-beam gradient force optical trap for dielectric particles. *Opt. Lett.* **1986**, *11*, 288–290. [CrossRef] [PubMed]
56. Franke-Arnold, S.; Allen, L.; Padgett, M. Advances in optical angular momentum. *Laser Photon. Rev.* **2008**, *2*, 299–313. [CrossRef]
57. Karimi, E.; Zito, G.; Piccirillo, B.; Marrucci, L.; Santamato, E. Hypergeometric-Gaussian modes. *Opt. Lett.* **2007**, *32*, 3053–3055. [CrossRef] [PubMed]
58. Jorge, K.C.; Riva, R.; Rodrigues, N.A.; Sakamoto, J.M.; Destro, M.G. Scattered light imaging method (SLIM) for characterization of arbitrary laser beam intensity profiles. *Appl. Opt.* **2014**, *53*, 4555–4564. [CrossRef]
59. Smyth, N.; Piccardi, A.; Alberucci, A.; Assanto, G. Highly nonlocal optical response: Benefit or drawback? *J. Nonl. Opt. Phys. Mat.* **2016**, *25*, 1650043. [CrossRef]
60. Laudyn, U.; Piccardi, A.; Kwasny, M.; Karpierz, M.; Assanto, G. Thermo-optic soliton routing in nematic liquid crystals. *Opt. Lett.* **2018**, *43*, 2296–2299. [CrossRef] [PubMed]
61. G. Assanto, G.; Khan, C.; Piccardi, A.; Smyth, N.F. Temperature control of nematicon trajectories. *Phys. Rev. E* **2019**, *100*, 062702. [CrossRef]
62. Jung, P.S.; Krolikowski, W.; Laudyn, U.A.; Trippenbach, M.; Karpierz, M.A. Supermode spatial optical solitons in liquid crystals with competing nonlinearities. *Phys. Rev. A* **2017**, *95*, 023820. [CrossRef]
63. Ramaniuk, A.; Trippenbach, M.; Jung, P.S.; Christodoulides, D.N.; W. Krolikowski, W.; Assanto, G. Scalar and vector supermode solitons owing to competing nonlocal nonlinearities. *Opt. Express* **2021**, *29*, 8015–8023. [CrossRef] [PubMed]